Thermochimica Acta, 230 (1993) 243–257
Elsevier Science Publishers B.V., Amsterdam
SSDI 0040-6031(93)01178-6

Spectroscopic and microscopic investigations of the thermal decomposition course of nickel oxysalts. Part 3. Nickel oxalate dihydrate

Seham A.A. Mansour

Chemistry Department, Faculty of Science, Minia University, El-Minia (Egypt)

(Received 23 February 1993; accepted 22 March 1993)

Abstract

The non-isothermal decomposition of nickel oxalate dihydrate (NiODH) in dynamic atmospheres of air or nitrogen has been investigated by means of TGA, DTA and DSC. The decomposition was followed by examining the decomposition products in each thermal reaction by IR spectroscopy, X-ray diffraction and electron microscopy. The dehydration reaction was endothermic in both atmospheres, giving rise to anhydrous nickel oxalate which still retained some water. On the other hand, the decomposition process was endothermic in air and exothermic in nitrogen. The final decomposition product in air was NiO, whereas in nitrogen the final product was found to be metallic nickel. Morphological changes throughout the decomposition were followed by SEM observations.

INTRODUCTION

Nickel oxysalts are considered as important precursors for the thermal production of NiO, which is well known as a powerful catalyst for a number of reactions, e.g. the oxidation of CO [1, 2], the decomposition of N_2O [3] and the oxidative dehydrogenation of aliphatic alcohols [4].

The NiO precursor investigated here is nickel oxalate dihydrate, the thermal decomposition of which has recently been subjected to several investigations [5–9]. However, most of these studies were carried out in a vacuum, an inert atmosphere or static air. Furthermore, there is no agreement on the decomposition temperatures under the same conditions [10] or the calculated non-isothermal kinetic parameters for the dehydration and decomposition steps [11–13], because of the methods adopted which are based on interpretation of a single TG curve.

The present comprehensive investigation of this reaction has been carried out under a dynamic atmosphere of either air or nitrogen to the onset of NiO production. Non-isothermal kinetic and thermodynamic parameters have been estimated adopting the method proposed by Ozawa [14, 15] using thermal analysis data at different heating rates. The de-

composition intermediates, as well as the final product, were characterized by infrared spectroscopy, X-ray diffractometry and scanning electron microscopy (SEM).

EXPERIMENTAL

Materials

The nickel oxalate dihydrate, $NiC_2O_4 \cdot 2H_2O$, used was a high purity (99.99%) Prolabo product. For simplicity, it will be denoted as NiODH. Solid decomposition products were obtained by calcination of NiODH at chosen temperatures in the range 290–500°C for 2 h in a static atmosphere of air, and were kept dry for further analyses.

Thermal analyses

TG and DTA analyses of NiODH were performed by heating at rates of 2, 5, 10 and 20 K min^{-1} up to 500°C in a dynamic atmosphere of air (30 cm^3 min^{-1}) using an automatic recording Shimadzu thermal analyser model 30 H (Japan). Typically, 10–15 mg portions of the test sample were used for the TG, and highly sintered α-Al_2O_3 was the reference material for DTA measurements. DSC data were recorded over the same range of temperature and at the same heating rates using the same apparatus, but under a dynamic atmosphere of nitrogen (30 cm^3 min^{-1}) to avoid oxidation. The heat of transition (28.24 J g^{-1} [16]) of Specpure indium metal (Johnson Matthey) at 157°C was used for DSC calibration.

Infrared spectroscopy

IR spectroscopic analyses were carried out over the frequency range 4000–300 cm^{-1}, at a resolution of 5.3 cm^{-1}, using a Perkin-Elmer model 580B double beam spectrophotometer (UK). The spectra were measured on thin (<20 mg cm^{-2}), lightly loaded (<1%) KBr-supported discs of the test samples.

X-ray diffractometry (XRD)

XRD analyses of NiODH and its calcination products were carried out using a Jeol diffractometer Model JSX-60 PA (Japan), with Ni-filtered Cu Kα radiation. The diffraction patterns of I/I_0 vs. d-spacing were compared with relevant ASTM standards [17].

Non-isothermal kinetic analysis of thermoanalytical data

From the TG and DTA curves, the temperatures (T_{max}) at which the weight was variant (TG) and invariant (DTA) were determined as a function of the heating rate (θ). The activation energy ΔE was calculated for each reaction from a plot of $\log \theta$ against $1/T_{max}$, according to the following relationship [14]

$$\Delta E = 2.19R[\mathrm{d} \log \theta / \mathrm{d}(1/T_{max})] \quad (1)$$

where R is the gas constant.

Calculation of the frequency factor A (min^{-1}) for the weight variant events was carried out assuming first-order reaction using the following relationship [18]

$$\log[-\log(1-C)/T^2] = \log AR/\theta\, \Delta E - \Delta E/2.303RT \quad (2)$$

where C is the fraction decomposed at T_{max}. The ΔE and A obtained were then used to calculate the rate constant k (min^{-1}) from the Arrhenius equation

$$k = A\mathrm{e}^{-\Delta E/RT} \quad (3)$$

The calculation of thermodynamic parameters

The enthalpy changes ΔH of the various reactions were determined directly from DSC traces using the following equation [18]

$$\Delta H = \frac{60BCq_m a}{m} \quad (4)$$

where B is the time base ($\mathrm{min\ cm}^{-1}$), C is the cell calibration coefficient, q_m is the Y-axis sensitivity ($\mathrm{J\ S}^{-1}\ \mathrm{cm}^{-1}$), a is the peak area (cm^{-2}) and m is the sample weight (g). ΔH was used to calculate the specific heat capacity (C_p) using the equation $C_p = \Delta H/\Delta T$, where $\Delta T = T_2 - T_1$, and T_1 and T_2 are the temperatures at beginning and end of the peak. The entropy change (ΔS) was calculated using the relationship $\Delta S = 2.303\ C_p \log(T_2/T_1)$ [19].

The activation energy (ΔE) was obtained from eqn. (1) by plotting $\log \theta$ against $1/T_m$ where T_m is the DSC peak temperature [14].

Electron microscopy

Examinations of the morphology and texture of NiODH and its calcination products were undertaken using a Jeol scanning electron microscope model 35 CF. Samples were mounted separately on aluminum stubs using a clear adhesive and pre-coated with gold–palladium in a

sputter coater to minimize the severe charging-up effects of the election on non-conductors.

For each sample, many crystals were examined and only features identified as being typical, reproducible and significant were photographed. The examples reproduced here were selected as being entirely representative of the textural changes that accompanied the reactions.

RESULTS AND DISCUSSION

TG and DTA curves for nickel oxalate dihydrate (NiODH) at heating rates of 2, 5, 10 and 20 K min^{-1} in a dynamic atmosphere of air are shown in Fig. 1. The TG curves indicate that NiODH loses weight in two

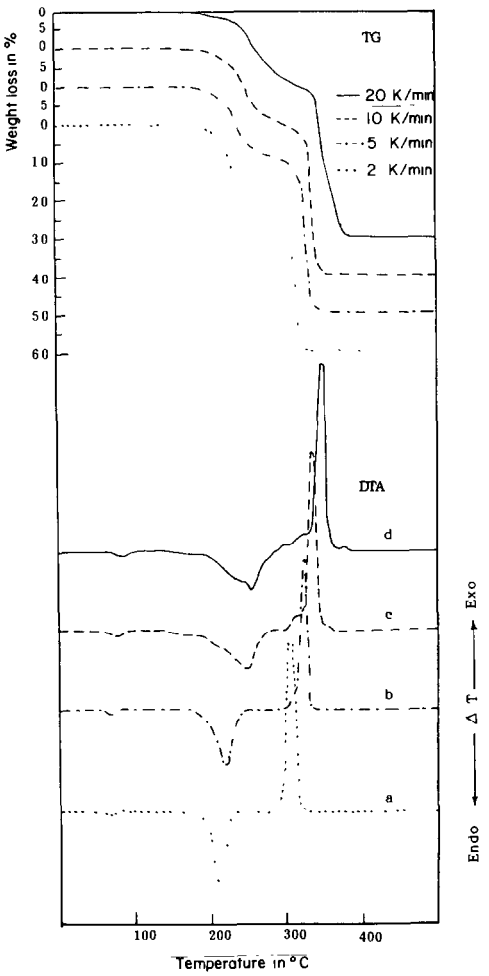

Fig. 1. TG and DTA curves of NiODH in dynamic (30 cm^3 min^{-1}) atmosphere of air at the heating rates indicated.

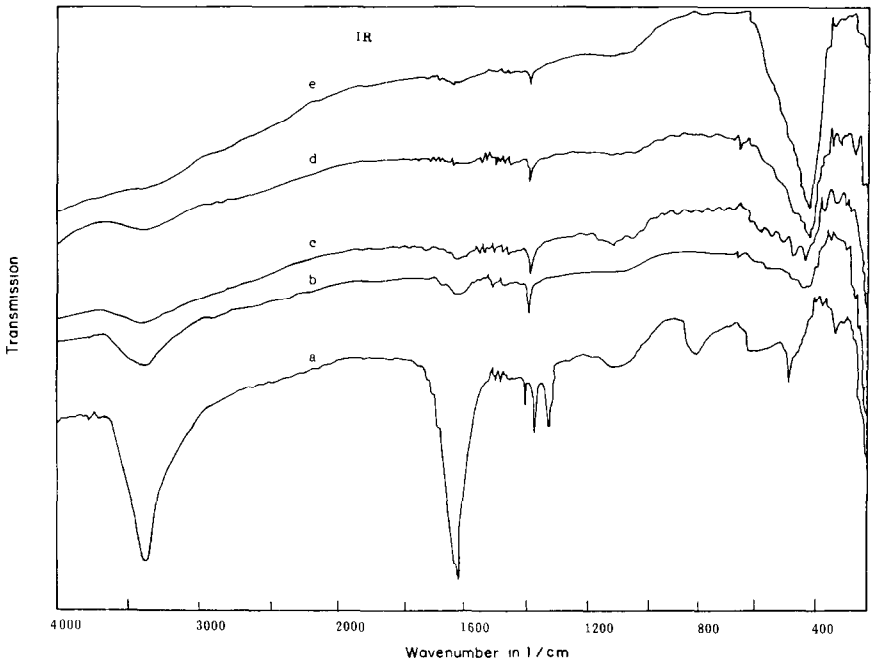

Fig. 2. The IR spectra of NiODH (a) and its calcination products at 290°C (b), 340°C (c), 375°C (d) and 500°C (e).

well-defined stages, in the ranges 175–300 and 300–360°C respectively, at a heating rate of 10 K min^{-1}. The corresponding DTA curve also at a heating rate of 10 K min^{-1} indicates that the first step is endothermic, with a maximum rate at 250°C, while the second step is exothermic with a maximimum rate at 340°C. These processes will be referred to as Stages I and II.

Figures 2 and 3 show the IR spectra and X-ray powder diffractograms respectively obtained for NiODH and its solid decomposition products.

The IR spectrum of the parent oxalate exhibits all the absorption bands of the coordinated oxalate group [14] at 1600 cm^{-1}, overlapped with H_2O bands at 1355, 1210, 820 and 485 cm^{-1}. Additional bands due to coordinated water at 3340, 1640, 725, 580 and 535 cm^{-1} are also present. The XRD trace (Fig. 3(a)) exhibits the lines characteristic of $NiC_2O_4 \cdot 2H_2O$ (ASTM card no. 25-581).

Figure 4 shows the TG and DTA curves for NiODH under a dynamic atmosphere of nitrogen (30 cm^3 min^{-1}) at a heating rate of 10 K min^{-1}. The corresponding TG and DTA curves in air at the same heating rate are included for comparison. The thermal behaviour in nitrogen shows that the two decomposition stages commence with two endothermic processes unlike that in air, in which the second process was exothermic.

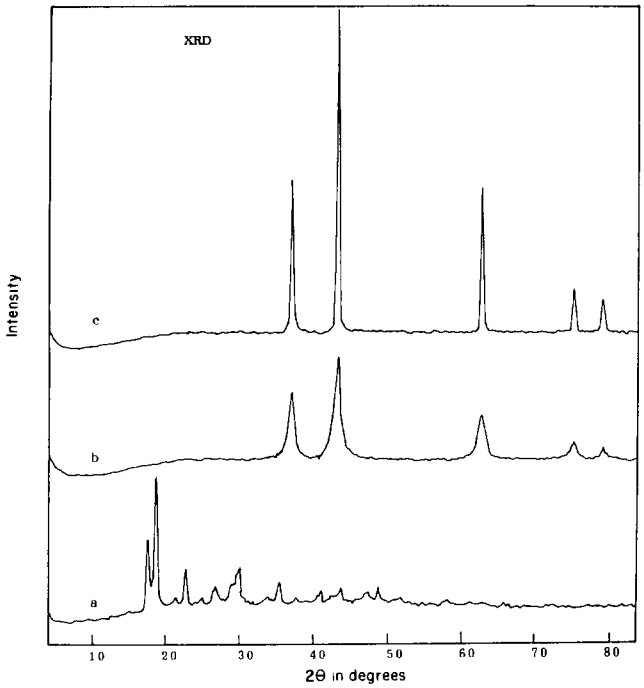

Fig. 3. X-ray powder diffractograms obtained for NiODH (a) and its calcination products at 375 (b) and 500°C (c).

The DSC traces during the decomposition of NiODH at heating rates of 5, 10 and 20 K min^{-1} in a nitrogen atmosphere are shown in Fig. 5. The curves exhibit two endothermic processes. Plots of log θ versus $1/T$ for the decomposition of NiODH from TG and DSC curves are presented in Figs. 6(a) and 6(b) respectively.

The non-isothermal kinetic parameters ΔE, k and A determined for stages I and II are listed in Table 1 for the TG and DTA curves. Table 2 gives the parameters for the DSC curves.

Characterization of the reactions and the decomposition products

Stage I

Stage I corresponds with 18% weight loss, a value which is slightly lower than that calculated (19.71%) for the dehydration of NiODH. The process is endothermic and starts at 175°C (at 10 K min^{-1}) with its maximum at 250°C.

The IR spectrum of the calcination product produced at 290°C (Fig. 2(b)) shows the H–OH absorption bands at 3450 cm^{-1} as well as those of the oxalate group. These observations indicate that a small amount of water is retained after the dehydration process. This water is probably occluded in

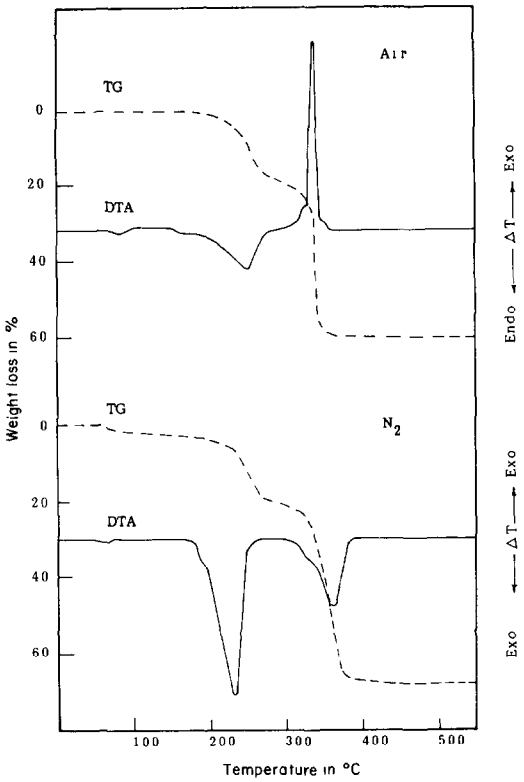

Fig. 4. The TG and DTA curves in N_2 and air (30 cm^3 min^{-1}) at 10 K min^{-1}.

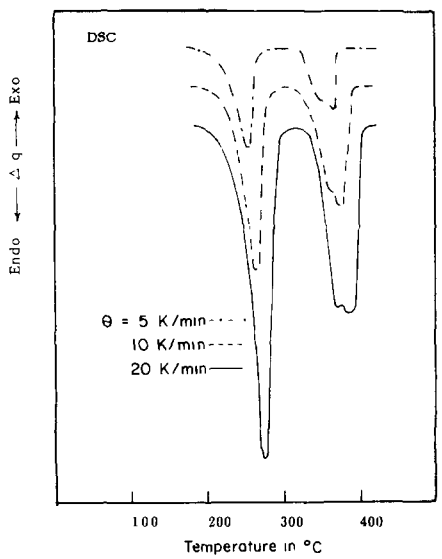

Fig. 5. DSC curves of NiODH at the heating rates (θ) indicated and in dynamic (30 cm^3 min^{-1}) atmosphere of dry nitrogen.

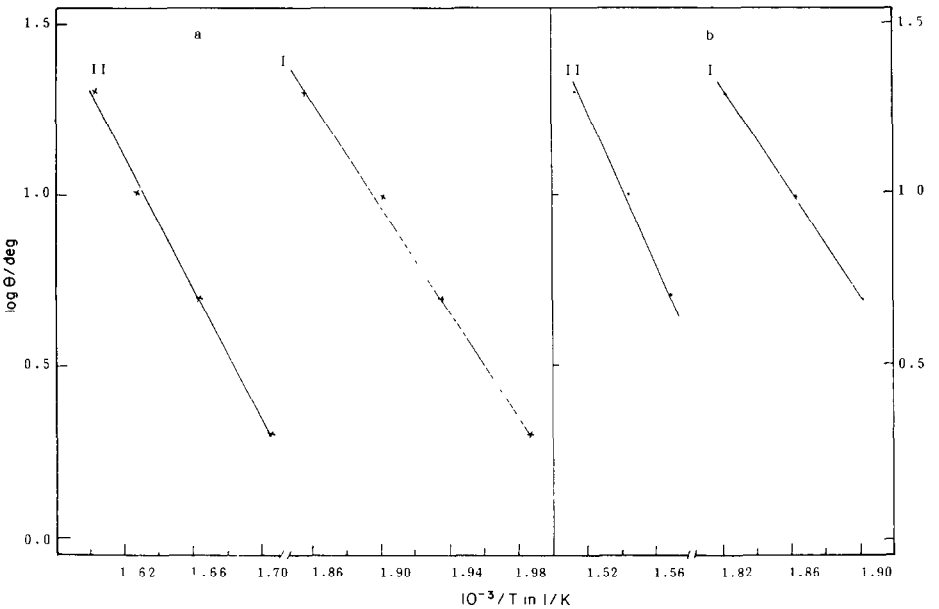

Fig. 6. Plots of $\log \theta$ vs. $1/T$ for stages I and II dervied from TG (a) and DSC (b) curves.

TABLE 1

Non-isothermal kinetic parameters of the various stages in the decomposition of NiODH (from TG and DTA data)

Stage	ΔE/kJ mol^{-1}	k/min^{-1}	log A/s^{-1}
I (endo)	123	1.7×10^{-2}	40
II (exo)	172	2.3×10^{-2}	14

TABLE 2

Non-isothermal kinetics and thermodynamic parameters of the stages in the decomposition of NiODH (DSC in dynamic atmosphere of nitrogen)

Stage	ΔE/kJ mol^{-1}	ln A/s^{-1}	k/min^{-1}	ΔH/kJ mol^{-1}	C_p/J g^{-1}	ΔS/J K ^{1}g^{-1}
I (endo)	136	29	0.56	63.5	4.4	0.83
II (endo)	206	37	0.59	48.5	4.5	0.55

the anhydrous crystals [20]. In this context, the X-ray diffractogram of the calcination product obtained at 290°C showed a less crystalline material than the parent NiODH. However, the product exhibited almost all of the lines characteristic of nickel oxalate (ASTM card no. 25-581).

It has been stated [11] that rigorous methods should be applied to estimate reliable kinetic parameters for the dehydration process, aimed particularly at minimizing the influence of water vapour. The present study was carried out under a dynamic atmosphere, and the influence of the water vapour is at a minimum. The non-isothermal dehydration activation energy value of 123 kJ mol^{-1} is very close to that reported by others [11].

Figure 4 shows that the dehydration process is endothermic, in the same temperature range, in both air and nitrogen. The TG curves indicate that at the end of this process the weight loss is the same in both atmospheres (18%).

Figure 5 shows that a well defined DSC peak corresponds with the dehydration process. The reaction kinetic and thermodynamic parameters are compiled in Table 2 for this process, and are in good agreement with the values obtained from the TG and DTA results as well as those reported [11]. The enthalpic change (ΔH) associated with the dehydration process amounts to 63 kJ mol^{-1}. This value is different from that of ΔE (136 kJ mol^{-1}). Such a difference indicates that the process is not adequately described by the Polany–Wigner relationship [21]. These findings agree with the reported data [11].

In conclusion, the results suggest that stage I involves the dehydration of NiODH, giving rise to a less well crystallized nickel oxalate containing a small amount of water occluded in the crystals. Furthermore, the calculated non-isothermal kinetic and thermodynamic parameters under dynamic atmospheres of air or nitrogen are consistent with one another, and the influence of water vapour is diminished by the gaseous flow.

Stage II

Figure 1 shows stage II as an exothermic process in air and bringing the total weight loss to 59.8% of the original weight the temperature range 300–360°C with a maximimum rate of weight loss at 340°C (Fig. 1(c)). Such a weight loss is close to that calculated for the transformation, $NiC_2O_4 \cdot 2H_2O \rightarrow NiO$.

The IR spectrum (Fig. 2(c)) of the calcination product at 340°C exhibits the H–OH band at 3450 cm^{-1} but of rather a low intensity. The spectrum also shows some characteristic oxalate absorption bands at 1640 cm^{-1}, but, ill defined absorption bands are present in the region of NiO absorption (viz. 700–300 cm^{-1}) [22].

The IR spectrum of the calcination product obtained at 375°C (Fig. 2(d)) after completion of decomposition exhibits mainly NiO absorption bands at 550, 425 and 325 cm^{-1} [22]. XRD of the product of calcination at 375°C

shows NiO lines (ASTM card no. 22-1189). Moreover, the IR spectrum Fig. 2(e)) and X-ray diffractogram (Fig. 3(c)) for the product of calcination at 500°C in air show bands of well-crystallized NiO.

These results reveal that stage II involves the removal of the water retained from the dehydration process (stage I). This occurs simultaneously with decomposition. The non-isothermal activation energy is calculated to be 172 kJ mol^{-1}, which is lower than determined elsewhere [13, 20] but higher than quoted by others [10]. Apparently, the activation energy for this stage seems to be a summation of those of the two simultaneous processes.

Stage II in a nitrogen atmosphere (see Fig. 4) is obviously endothermic with a peak rate at 360°C and covering a wider range of temperature (300–390°C) than in air. The total weight loss was 68% and equal to that for transformation $NiC_2O_4 \cdot 2H_2O \rightarrow Ni$ (ca. 67.8%).

The DSC curve of stage II, presented in Fig. 5, shows an endothermic process with a peak at 375°C at $\theta = 10\,K\,min^{-1}$ and with a shoulder at 355°C. The activation energy from the DSC results, see Table 2, is 206 kJ mol^{-1}.

It has been reported [8] that the decomposition of bivalent metal oxalates in nitrogen can be described by the equations

$$MC_2O_4 = MO + CO + CO_2 \quad (6)$$

$$MC_2O_4 = M + 2CO_2 \quad (7)$$

Furthermore, according to thermodynamic considerations, it has been stated [8] that under equilibrium conditions reaction (6) predominates over reaction (7) and vice versa.

For the present study, i.e. under a dynamic atmosphere of nitrogen, equilibrium conditions are obviously not established; this leads to the conclusion that reaction (7) predominates under the conditions used. On the other hand, the shoulder on the DSC curves could be attributed to different allotropic modifications of the nickel metal. These findings disagree with those of Nikumbh et al. [10], who claimed that NiO is the sole final thermal decomposition product of nickel oxalate dihydrate under a dynamic nitrogen atmosphere. Furthermore, several authors [8, 13, 20, 23] concluded that the decomposition of NiODH in a nitrogen atmosphere yields metallic nickel, which confirms the results obtained.

Electron microscopic examination

SEM was carried out to correlate the morphological changes accompanying the decomposition of NiODH with the corresponding physicochemical characterization. Electron micrographs were taken of the parent oxalate and its calcination products.

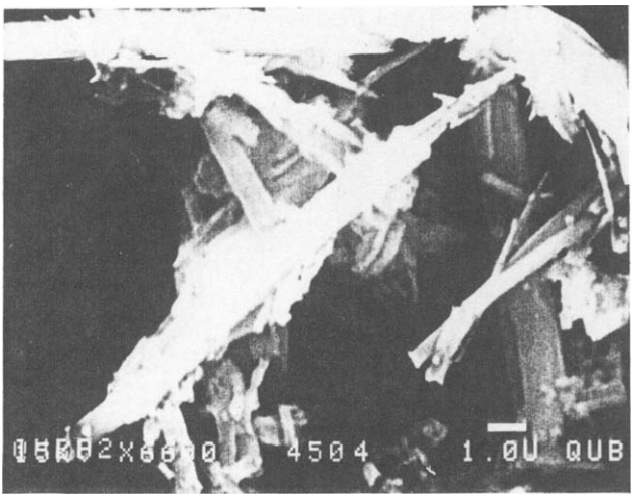

Fig. 7. Scanning electron micrograph of the parent NiODH.

The parent salt was composed of fine needle-like crystals with a smooth skin. These crystals had a range of different sizes and small fragments appeared to result from the crystals breaking irregularly. Typical crystals are shown in Fig. 7.

No appreciable particle size reduction was observed as a result of the dehydration process. However, the skin of the sample heated at 290°C, corresponding to dehydrated crystals, was wrinkled and clear grooves appeared on them; see Fig. 8. This is in accordance with XRD results in that the dehydrated salt was crystalline in nature.

When the temperature had reached 320°C (Figs. 9(a) and 9(b)), the grooves widened and the crystals seemed slightly distorted and penetrated

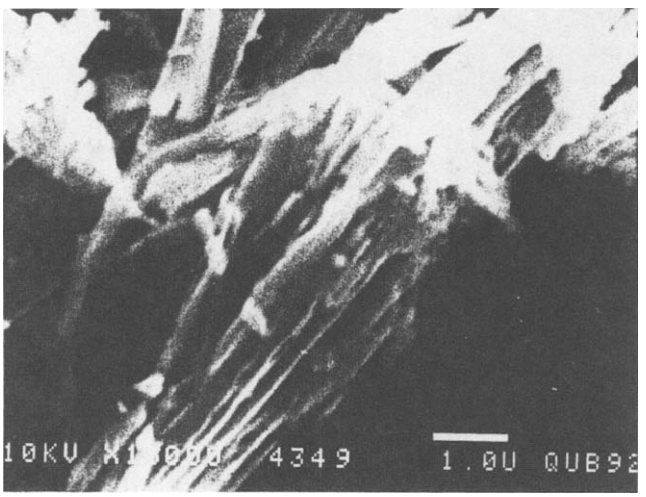

Fig. 8. Scanning electron micrograph of NiODH calcined at 290°C.

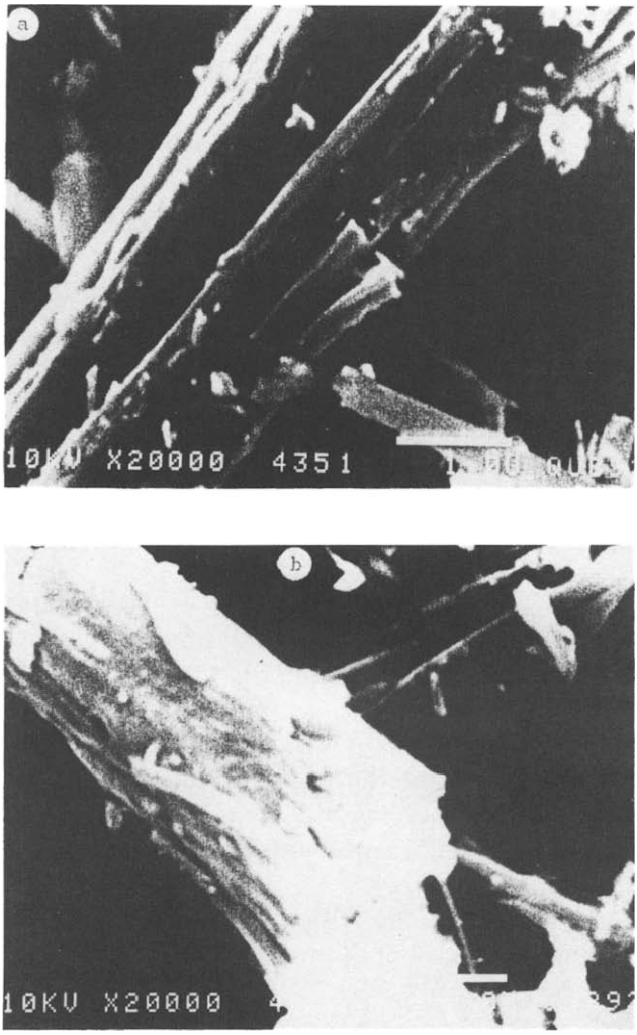

Fig. 9. (a) Scanning electron micrograph of NiODH heated at 320°C. (b) Light crushing of NiODH heated at 320°C revealed an internal slab-like structure.

with parallel and irregular cracks (Fig. 9(a)). Partial crushing of the crystals revealed an internal slab-like structure (Fig. 9(b)). On raising the temperature to 340°C, decomposition seemed to proceed along these cracks with the creation of nuclei of a new product; see Fig. 10. For the same product, Fig. 11 shows that nucleation appears as nodules, and this is undoubtedly associated with the onset of decomposition.

Finally, Figs. 12(a) and 12(b) show the micrographs of the decomposed salt at 500°C. These indicate remarkable phenomenological changes relative to the parent as well as the dehydrated salt. Figure 12(a) shows clearly the disappearance of the crystal faces and the disruption of the

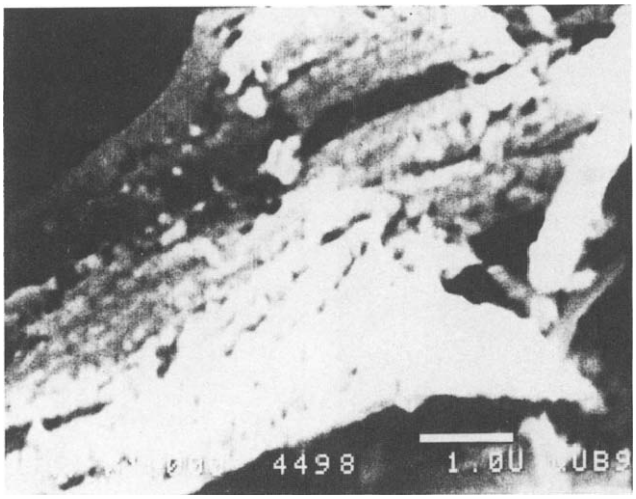

Fig. 10. Scanning electron micrograph of NiODH calcined at 340°C.

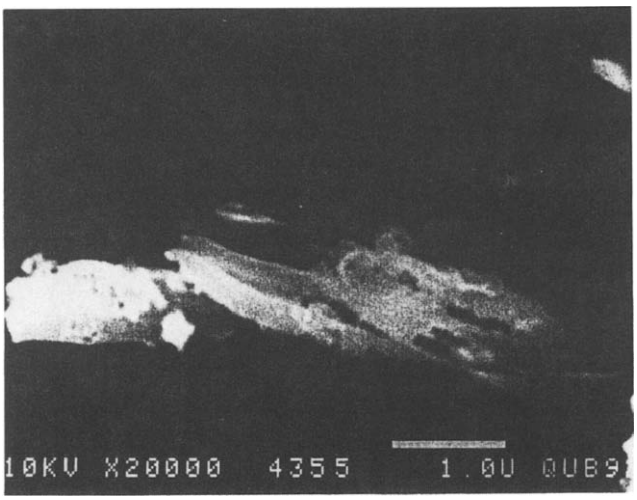

Fig. 11. Nucleation of the decomposition product at 340°C.

crystal structure of the parent salt. The final decomposition product consists of particles of aggregates of very fine crystals, as seen in Fig. 12(b).

CONCLUSIONS

The present study leads to the following conclusions.

1. The dehydration of $NiC_2O_4 \cdot 2H_2O$ in air or nitrogen takes place through one endothermic step, yielding anhydrous nickel oxalate crystals occluding a small portion of water, which was detected by IR spectroscopy.

2. The non-isothermal kinetic and thermodynamic parameters for the dehydration step are reliable, since the water vapour has no effect.

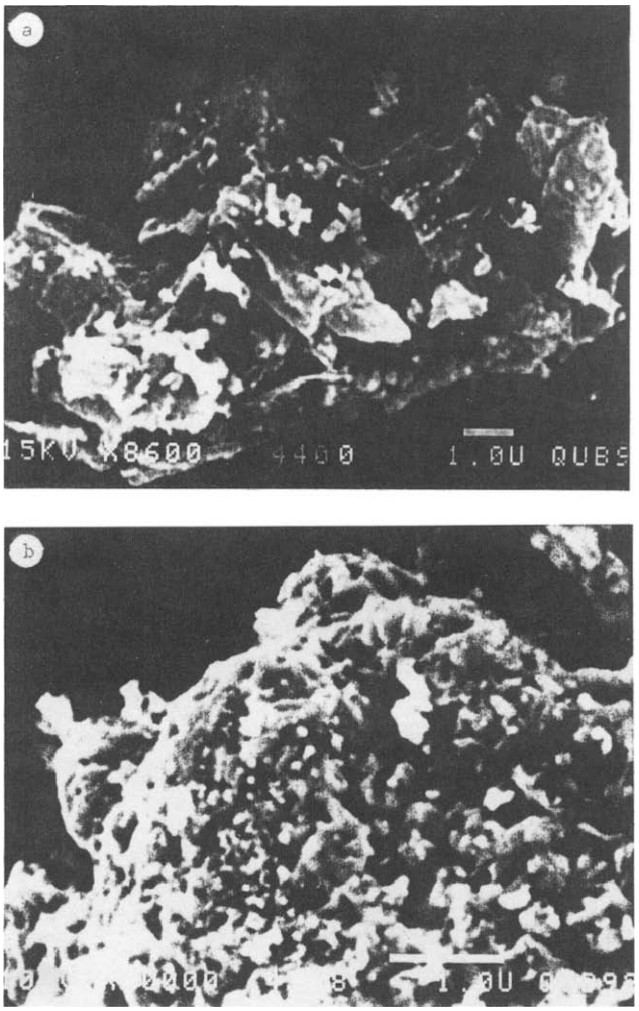

Fig. 12. Electron micrographs of the final decomposition product.

3. The final product of the decomposition in a dynamic atmosphere of air was NiO, whereas in a dynamic nitrogen atmosphere the product was metallic nickel.

4. Remarkable phenomenological and morphological changes were found to accompany the decomposition process.

ACKNOWLEDGEMENTS

It is a pleasure to thank the Queen's University of Belfast, particularly the staff of the Electron Microscope Unit, for assistance in obtaining the electron micrographs. Thanks are also due to the Egyptian Government for the grant of a Fellowship.

REFERENCES

1 J. Deren, B. Russer, J. Nowotny, G. Rog and J. Sloczynski, J. Catal., 34 (1974) 124.
2 G. El-Shobaky, P.C. Gravelle and S.J. Teichner, Adv. Chem. Ser., 67 (1988) 292.
3 M.I. Zaki, S.A.A. Mansour and R.B. Fahim, Surf. Technol., 25 (1985) 287.
4 J. Gunningham, B.K. Hodnelt, M. Ilyas, J. Tobin and E.L. Leahy, Discuss. Faraday Soc., 72 (1981) 283.
5 J. Robin, Bull. Soc. Chim. Fr., (1953) 1078.
6 K. Kawagaki, J. Chem. Soc. Jpn., 72 (1951) 1079.
7 R. David, Bull. Soc. Chim. Fr., (1960) 719.
8 D. Dollimore, D.L. Griffiths and D. Nicholson, J. Chem. Soc., (1963) 2617.
9 C. Duval, Inorganic Thermogravimetric Analysis, Elsevier, Amsterdam, 1963.
10 A.K. Nikumbh, A.E. Athare and V.B. Rault, Thermochim. Acta, 186 (1991) 217.
11 W.E. Brown, D. Dollimore and A.K. Galwey, in C.H. Bamford and C.E.H. Tripper (Eds.), Chemical Kinetics, Vol. 22, Reactions in the Solid State, Elsevier, Amsterdam, 1980, pp. 134–135.
12 A. Alloun and C.G.R. Nair, Thermochim. Acta, 921 (1985) 767.
13 W.J. Young and B. Hall, Thermochim. Acta, 147 (1989) 251.
14 T. Ozawa, J. Therm. Anal., 2 (1970) 301.
15 T. Ozawa, J. Therm. Anal., 9 (1976) 369.
16 C.R. Weast (Ed.), Handbook of Chemistry and Physics, CRC Press, Boca Raton, FL 62nd edn., 1982.
17 W. Frank et al. (Eds.), Powder Diffraction File for Inorganic Phase, International Center for Diffraction Data, Philadelphia, PA, 1981.
18 K.F. Baker, Du Pont Instruments, Thermal Analysis Application Brief, No. TA-53.
19 C. Heald and A.C.K. Smith, Applied Physical Chemistry, Macmillan, London, 1992, pp. 20–40.
20 D. Dollimore, in R.C. Mackenzie (Ed.), Differential Thermal Analysis, Academic Press, London, 1970, pp. 396–423.
21 M. Polanyi and E. Wigner, Z. Phys. Chem. Abt. A, 139 (1928) 439.
22 F.F. Bently, L.D. Smithson and A.L. Rozek (Eds.), Infrared Spectra and Characteristic Frequencies $\approx$700–300 cm^{-1}, Wiley, New York, 1968.
23 K. Nagaso, K. Sato and N. Tanaka, Bull. Chem. Soc. Jpn., 48 (1975) 439.